Z. Angew. Math. Phys. 66 (2015), 3645–3661

0044-2275/15/063645-17
published online September 1, 2015
DOI 10.1007/s00033-015-0576-0

Zeitschrift für angewandte Mathematik und Physik ZAMP

Interaction of a screw dislocation with an interface and a nanocrack incorporating surface elasticity

Xu Wang

Abstract. We study the anti-plane deformations of a linearly elastic bimaterial. One phase of the bimaterial is weakened by a finite crack with surface elasticity perpendicular to the interface and is also subjected to a screw dislocation. The surface elasticity is incorporated by using a version of the continuum-based surface/interface model of Gurtin and Murdoch. By considering a distribution of screw dislocations and line forces on the crack, the interaction problem is reduced to two decoupled first-order Cauchy singular integro-differential equations, which can be numerically solved by means of the Chebyshev polynomials and the collocation method. The associated problem of a mode III Zener–Stroh crack perpendicular to a bimaterial interface is also solved.

Mathematics Subject Classification. 30D10 · 45E05 · 45J05 · 74R10 · 74B05 · 74S70 · 74M25.

Keywords. Surface elasticity · Bimaterial · Griffith crack · Zener–Stroh crack · Screw dislocation · Anti-plane deformations · Green's function method · Singular integro-differential equations · Image force.

1. Introduction

Interaction between singularities, cracks and interfaces is always an intriguing, whereas challenging problem in micromechanics [21,22]. The solution to the singularity–interface problem (a singularity in an elastically isotropic or anisotropic bimaterial) can be obtained by using the method of analytical continuation [21,22] or the method of image [4,23]. The singularity–crack interaction problem can be solved by means of the complex variable method [17,21,22,31,32]. The crack–interface interaction problem (a crack in one phase of a bimaterial) can be reduced to the solution of singular integral equations by simulating the crack by a distribution of dislocations [5,7,30]. Very recently, there has been a growing interest in augmenting the classical linear elastic fracture mechanics (LEFM) with the Gurtin–Murdoch surface mechanics with a goal to study the mechanical behaviors of cracked structures at the nanoscale (see, for example, [1,11–16,25–29]). Roughly speaking, the Gurtin–Murdoch surface model is equivalent to the assumption of a surface as a thin and stiff solid film of separate elasticity perfectly bonded to the bulk [3,18,20]. When the Gurtin–Murdoch surface elasticity is incorporated into the mechanics of crack faces, an array of both dislocations and line forces is required to simulate the crack [25–27,29].

Analytically studied in this work is the interaction problem of a screw dislocation near a finite crack with surface elasticity, which is perpendicular to a bimaterial interface. The crack is simulated by a distribution of screw dislocations and anti-plane line forces. From the Green's function solution for a bimaterial subjected to a screw dislocation and a line force not located at the interface [4,24], we know that the screw dislocation and line force are under the stress field of their own images caused by the bimaterial interface. The interaction problem is finally reduced to two decoupled first-order Cauchy singular integro-differential equations that are numerically solved by means of the Gauss–Chebyshev integration formula [6], the Chebyshev polynomials and the collocation method. Detailed numerical results are presented to demonstrate the elastic mismatch of the bimaterial, the surface elasticity and the positions of the screw dislocation and the crack on the dislocation and line force densities over the crack, and on the material force acting on the screw dislocation.

2. Basic formulation

In this section, the basic formulations for the coupled bulk and surface elasticity will be briefly reviewed for the completeness of the paper.

2.1. The bulk elasticity

In the absence of body forces, the equations of equilibrium and the stress–strain law for a linearly elastic, homogeneous and isotropic bulk solid in a Cartesian coordinate system $x_i (i = 1, 2, 3)$ are

$$\sigma_{ij,j} = 0, \quad \sigma_{ij} = 2\mu\varepsilon_{ij} + \lambda\varepsilon_{kk}\delta_{ij}, \quad \varepsilon_{ij} = \frac{1}{2}(u_{i,j} + u_{j,i}), \tag{1}$$

where λ and μ are Lame constants, σ_{ij} and ε_{ij} are, respectively, the stress and strain tensors in the bulk material, u_i is the i-th component of the displacement vector $\mathbf{u}$, δ_{ij} is the Kronecker delta.

For the anti-plane shear deformations of an isotropic elastic material, the two shear stress components σ_{31} and σ_{32}, the out-of-plane displacement $w = u_3(x_1, x_2)$ can be expressed in terms of a single analytic function $h(z)$ of the complex variable $z = x_1 + \mathrm{i}x_2$ as

$$\sigma_{32} + \mathrm{i}\sigma_{31} = \mu h'(z), w = \mathrm{Im}\{h(z)\}. \tag{2}$$

2.2. The surface elasticity

The equilibrium conditions on the surface incorporating interface/surface elasticity can be expressed as [8–10,19]

$$\begin{aligned} &[\sigma_{\alpha j} n_j \underline{e}_\alpha] + \sigma^s_{\alpha\beta,\beta}\underline{e}_\alpha = 0, \quad &&\text{(tangential direction)} \\ &[\sigma_{ij} n_i n_j] = \sigma^s_{\alpha\beta}\kappa_{\alpha\beta}, &&\text{(normal direction)} \end{aligned} \tag{3}$$

where $\alpha, \beta = 1, 3; n_i$ is the unit normal vector to the surface, $[*]$ denotes the jump of the quantities across the surface, $\sigma^s_{\alpha\beta}$ is the surface stress tensor and $\kappa_{\alpha\beta}$ is the curvature tensor of the surface. In addition, the constitutive equations on the isotropic surface are given by

$$\sigma^s_{\alpha\beta} = \sigma_0\delta_{\alpha\beta} + 2(\mu^s - \sigma_0)\varepsilon^s_{\alpha\beta} + (\lambda^s + \sigma_0)\varepsilon^s_{\gamma\gamma}\delta_{\alpha\beta} + \sigma_0\nabla_s\mathbf{u}, \tag{4}$$

where $\varepsilon^s_{\alpha\beta}$ is the surface strain tensor, σ_0 is the surface tension, λ^s and μ^s are the two surface Lame parameters, ∇_s is the surface gradient.

3. The interface–dislocation–crack interaction problem

As shown in Fig. 1, we consider a bimaterial composed of two perfectly bonded half-planes: $S_1 : x_1 > 0, -\infty < x_2 < +\infty$ and $S_2 : x_1 < 0, -\infty < x_2 < +\infty$. The right half-plane S_1 is weakened by a finite crack $[d - a \le x_1 \le d + a], (x_2 = 0)$ perpendicular to the bimaterial interface and is subjected to a screw dislocation with Burgers vector b_z located at $z = z_0, \mathrm{Re}\{z_0\} > 0$ outside the crack. As shown in Fig. 1, $z_0 - d = r\exp(\mathrm{i}\theta)$ where θ is the dislocation angle and r is the dislocation distance. Throughout the paper, the subscripts 1 and 2 or the superscripts (1) and (2) are used to denote the quantities in S_1 and S_2.

From Eq. (3), the boundary conditions on the crack surface can be written as

$$\sigma^s_{13,1} + (\sigma_{23})^+ - (\sigma_{23})^- = 0, \quad \text{on the upper crack face,} \tag{5a}$$

$$\sigma^s_{13,1} + (\sigma_{23})^+ - (\sigma_{23})^- = 0, \quad \text{on the lower crack face,} \tag{5b}$$

where $(\sigma_{23})^-$ in Eq. (5a) and $(\sigma_{23})^+$ in Eq. (5b) are zero. By using the constitutive relations in Eq. (4) and assuming a coherent interface ($\varepsilon^s_{\alpha\beta} = \varepsilon_{\alpha\beta}$), the following can be further obtained from Eqs.(5a,b)

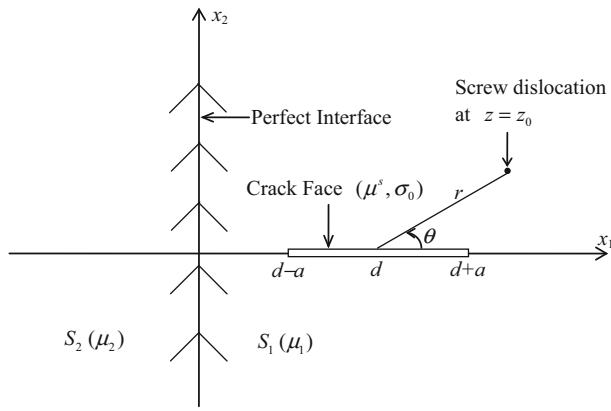

FIG. 1. A screw dislocation interacting with a bimaterial interface and a finite crack with surface elasticity perpendicular to the interface

$$(\sigma_{23})^+ = -(\mu^s - \sigma_0)u^+_{3,11}, \quad \text{on the upper crack face,} \tag{6}$$

$$(\sigma_{23})^- = +(\mu^s - \sigma_0)u^-_{3,11}, \quad \text{on the lower crack face,} \tag{7}$$

which are equivalent to

$$\begin{aligned}(\sigma_{23})^+ + (\sigma_{23})^- &= -(\mu^s - \sigma_0)(u^+_{3,11} - u^-_{3,11}),\\ (\sigma_{23})^+ - (\sigma_{23})^- &= -(\mu^s - \sigma_0)(u^+_{3,11} + u^-_{3,11}).\end{aligned} \tag{8}$$

Below, the interface–dislocation–crack interaction problem will be formulated by considering a distribution of screw dislocations with density $b(x_1)$, and line forces with density $f(x_1)$ on the crack. The two analytic functions $h_1(z)$ defined in the right half-plane and $h_2(z)$ defined in the left half-plane then take the following form

$$\begin{aligned}h_1(z) = {}& \frac{1}{2\pi}\int_{d-a}^{d+a}\left[b(\xi) - \mathrm{i}\mu_1^{-1}f(\xi)\right]\ln(z-\xi)\mathrm{d}\xi + \frac{K}{2\pi}\int_{d-a}^{d+a}\left[b(\xi) + \mathrm{i}\mu_1^{-1}f(\xi)\right]\ln(z+\xi)\mathrm{d}\xi\\ &+\frac{b_z}{2\pi}\ln(z-z_0) + \frac{Kb_z}{2\pi}\ln(z+\bar{z}_0), \quad \mathrm{Re}\,\{z\} > 0;\\ h_2(z) = {}& \frac{1-K}{2\pi}\int_{d-a}^{d+a}\left[b(\xi) - \mathrm{i}\mu_1^{-1}f(\xi)\right]\ln(z-\xi)\mathrm{d}\xi + \frac{(1-K)b_z}{2\pi}\ln(z-z_0), \quad \mathrm{Re}\,\{z\} < 0;\end{aligned} \tag{9}$$

where $K = (\mu_2 - \mu_1)/(\mu_1 + \mu_2), -1 \le K \le 1$ is the mismatch parameter for the bimaterial. A positive value of K means that material 2 is harder than material 1, whereas a negative value of K implies that material 2 is softer than material 1. $K = 1$ when material 2 is rigid, $K = -1$ when material 2 is void, $K = 0$ when the two phases are identical.

It is then deduced from the above expression that

$$\begin{aligned}h_1'^+(x_1) = {}& -\frac{\mathrm{i}b(x_1) + \mu^{-1}f(x_1)}{2} + \frac{1}{2\pi}\int_{d-a}^{d+a}\frac{b(\xi) - \mathrm{i}\mu^{-1}f(\xi)}{x_1 - \xi}\mathrm{d}\xi + \frac{K}{2\pi}\int_{d-a}^{d+a}\frac{b(\xi) + \mathrm{i}\mu^{-1}f(\xi)}{x_1 + \xi}\mathrm{d}\xi\\ &+\frac{b_z}{2\pi}\frac{1}{x_1 - z_0} + \frac{Kb_z}{2\pi}\frac{1}{x_1 + \bar{z}_0},\end{aligned} \tag{10}$$

$$h_1'^{-}(x_1)=\frac{\mathrm{i}b(x_1)+\mu^{-1}f(x_1)}{2}+\frac{1}{2\pi}\int_{d-a}^{d+a}\frac{b(\xi)-\mathrm{i}\mu^{-1}f(\xi)}{x_1-\xi}\mathrm{d}\xi+\frac{K}{2\pi}\int_{d-a}^{d+a}\frac{b(\xi)+\mathrm{i}\mu^{-1}f(\xi)}{x_1+\xi}\mathrm{d}\xi$$
$$+\frac{b_z}{2\pi}\frac{1}{x_1-z_0}+\frac{Kb_z}{2\pi}\frac{1}{x_1+\bar{z}_0},\tag{11}$$

where $d-a<x_1<d+a$; the superscript "+"' means the limiting value by approaching the crack from the upper half-plane, the superscript "−" means the limiting value by approaching the crack from the lower half-plane. Through satisfaction of the boundary conditions in Eq. (8), we can obtain the following two decoupled hyper-singular integro-differential equations

$$-\frac{\mu_1}{\pi}\int_{d-a}^{d+a}\frac{b(\xi)}{\xi-x_1}\mathrm{d}\xi+\frac{K\mu_1}{\pi}\int_{d-a}^{d+a}\frac{b(\xi)}{\xi+x_1}\mathrm{d}\xi+\frac{\mu_1 b_z}{\pi}\mathrm{Re}\left\{\frac{1}{x_1-z_0}\right\}+\frac{K\mu_1 b_z}{\pi}\mathrm{Re}\left\{\frac{1}{x_1+z_0}\right\}$$
$$=(\mu^s-\sigma_0)b'(x_1),\quad d-a<x_1<d+a,\tag{12}$$

$$f(x_1)=(\mu^s-\sigma_0)\left[\frac{1}{\pi\mu_1}\int_{d-a}^{d+a}\frac{f(\xi)}{(x_1-\xi)^2}\mathrm{d}\xi-\frac{K}{\pi\mu_1}\int_{d-a}^{d+a}\frac{f(\xi)}{(x_1+\xi)^2}\mathrm{d}\xi\right.$$
$$\left.-\frac{b_z}{\pi}\mathrm{Im}\left\{\frac{1}{(x_1-z_0)^2}\right\}+\frac{Kb_z}{\pi}\mathrm{Im}\left\{\frac{1}{(x_1+z_0)^2}\right\}\right],\quad d-a<x_1<d+a.\tag{13}$$

Equation (13) can be recast into the following equivalent form

$$\int_{d-a}^{x_1}f(\xi)\mathrm{d}\xi=(\mu^s-\sigma_0)\left[\frac{1}{\pi\mu_1}\int_{d-a}^{d+a}\frac{f(\xi)}{\xi-x_1}\mathrm{d}\xi+\frac{K}{\pi\mu_1}\int_{d-a}^{d+a}\frac{f(\xi)}{\xi+x_1}\mathrm{d}\xi+\frac{b_z}{\pi}\mathrm{Im}\left\{\frac{1}{x_1-z_0}\right\}\right.$$
$$\left.-\frac{Kb_z}{\pi}\mathrm{Im}\left\{\frac{1}{x_1+z_0}\right\}\right],d-a<x_1<d+a.\tag{14}$$

It is deduced from Eqs. (10) and (11) that

$$\Delta w=w^+-w^-=-\int_{d-a}^{x_1}b(\xi)\mathrm{d}\xi,\sigma_{32}^+-\sigma_{32}^-=-f(x_1),d-a<x_1<d+a.\tag{15}$$

The requirements of the single valuedness of the displacement and the balance of force for a contour surrounding the crack surface lead to

$$\int_{d-a}^{d+a}b(\xi)\mathrm{d}\xi=0,\int_{d-a}^{d+a}f(\xi)\mathrm{d}\xi=0.\tag{16}$$

The original interaction problem has been reduced to two decoupled first-order Cauchy singular integro-differential Eqs. (12) and (14) together with the two auxiliary conditions in Eq. (16).

We set $x=(x_1-d)/a$ and $t=(\xi-d)/a$ in Eqs. (12), (14) and (16). For convenience, we write $b(x)=b(x_1)$ and $f(x)=f(x_1)$. Consequently, Eqs. (12), (14) and (16) can be written into the following normalized form

$$-\frac{1}{\pi}\int_{-1}^{1}\frac{\hat{b}(t)}{t-x}\mathrm{d}t+\frac{K}{\pi}\int_{-1}^{1}\frac{\hat{b}(t)}{x+t+2\hat{d}}\mathrm{d}t+\frac{1}{\pi}\mathrm{Re}\left\{\frac{1}{x-\hat{z}_0}\right\}+\frac{K}{\pi}\mathrm{Re}\left\{\frac{1}{x+\hat{z}_0+2\hat{d}}\right\}$$
$$=S_e\hat{b}'(x),\ -1<x<1,\tag{17}$$

$$\frac{1}{\pi}\int_{-1}^{1}\frac{\hat{f}(t)}{t-x}\mathrm{d}t+\frac{K}{\pi}\int_{-1}^{1}\frac{\hat{f}(t)}{x+t+2\hat{d}}\mathrm{d}t-\frac{1}{S_e}\int_{-1}^{x}\hat{f}(t)\mathrm{d}t$$
$$=-\frac{1}{\pi}\mathrm{Im}\left\{\frac{1}{x-\hat{z}_0}\right\}+\frac{K}{\pi}\mathrm{Im}\left\{\frac{1}{x+\hat{z}_0+2\hat{d}}\right\},\ -1<x<1, \tag{18}$$

$$\int_{-1}^{1}\hat{b}(t)\mathrm{d}t=0,\int_{-1}^{1}\hat{f}(t)\mathrm{d}t=0, \tag{19}$$

where

$$\hat{b}(x)=\frac{ab(x)}{b_z},\quad \hat{f}(x)=\frac{af(x)}{\mu_1 b_z},\quad S_e=\frac{\mu^s-\sigma_0}{a\mu_1},\quad \hat{z}_0=\frac{z_0-d}{a},\quad \hat{d}=\frac{d}{a}. \tag{20}$$

A comparison of Eqs. (17) and (18) with the corresponding results by Wang and Fan [26] reveals that additional regular integrals and additional loading terms are present due to the elastic mismatch of the two phases ($K\neq 0$). The appearance of the regular integrals will make the two integro-differential equations more difficult to be solved.

4. Solution of the singular integro-differential equations

By using the Gauss–Chebyshev integration formula [6], Eq. (17) can be approximately written into

$$-\frac{1}{\pi}\int_{-1}^{1}\frac{\hat{b}(t)}{t-x}\mathrm{d}t+\frac{K}{M}\sum_{j=1}^{M}\frac{\sqrt{1-(t_j)^2}\hat{b}(t_j)}{x+t_j+2\hat{d}}+\frac{1}{\pi}\mathrm{Re}\left\{\frac{1}{x-\hat{z}_0}\right\}+\frac{K}{\pi}\mathrm{Re}\left\{\frac{1}{x+\hat{z}_0+2\hat{d}}\right\}=S_e\hat{b}'(x), \tag{21}$$

where

$$t_j=\cos\left(\frac{\pi(2j-1)}{2M}\right),\ j=1,2,\ldots,M. \tag{22}$$

By applying the following inverse operator to Eq. (21) [2,12]

$$T^{-1}\psi(x)=\frac{1}{\pi\sqrt{1-x^2}}\int_{-1}^{1}\psi(t)\mathrm{d}t-\frac{1}{\pi^2\sqrt{1-x^2}}\int_{-1}^{1}\frac{\sqrt{1-t^2}\psi(t)}{t-x}\mathrm{d}t,\quad -1<x<1, \tag{23}$$

we obtain

$$\hat{b}(x)=\frac{1}{\pi\sqrt{1-x^2}}\int_{-1}^{1}\hat{b}(t)\mathrm{d}t$$
$$-\frac{1}{\pi\sqrt{1-x^2}}$$
$$\times\int_{-1}^{1}\frac{\sqrt{1-t^2}\left[-S_e\hat{b}'(t)+\frac{K}{M}\sum_{j=1}^{M}\frac{\sqrt{1-(t_j)^2}\hat{b}(t_j)}{t+t_j+2\hat{d}}+\frac{1}{\pi}\mathrm{Re}\left\{\frac{1}{t-\hat{z}_0}\right\}+\frac{K}{\pi}\mathrm{Re}\left\{\frac{1}{t+\hat{z}_0+2\hat{d}}\right\}\right]}{t-x}\mathrm{d}t,-1<x<1. \tag{24}$$

In view of the first condition in Eq. (19), the above can be simplified to

$$\hat{b}(x) = -\frac{1}{\pi\sqrt{1-x^2}} \times \int_{-1}^{1} \frac{\sqrt{1-t^2}\left[-S_e\hat{b}'(t) + \frac{K}{M}\sum_{j=1}^{M}\frac{\sqrt{1-(t_j)^2}\hat{b}(t_j)}{t+t_j+2\hat{d}} + \frac{1}{\pi}\mathrm{Re}\left\{\frac{1}{t-\hat{z}_0}\right\} + \frac{K}{\pi}\mathrm{Re}\left\{\frac{1}{t+\hat{z}_0+2\hat{d}}\right\}\right]}{t-x}\mathrm{d}t, \quad -1<x<1. \tag{25}$$

The unknown density function $\hat{b}(x)$ is approximated as

$$\hat{b}(x) = \sum_{m=0}^{N} c_m T_m(x), \tag{26}$$

where $T_m(x)$ represents the mth Chebyshev polynomial of the first kind, and $c_m, m = 0, 1, 2, \ldots, N$ are $N+1$ unknown coefficients.

Inserting Eq. (26) into Eq. (25), and utilizing the following identities

$$\frac{\mathrm{d}T_m(x)}{\mathrm{d}x} = mU_{m-1}(x), \int_{-1}^{1}\frac{U_m(t)\sqrt{1-t^2}}{t-x}\mathrm{d}t = -\pi T_{m+1}(x), \tag{27}$$

$$\int_{-1}^{1}\frac{\sqrt{1-t^2}}{(t-x)(t-\hat{z}_0)}\mathrm{d}t = -\pi\left(1+\frac{\sqrt{\hat{z}_0^2-1}}{x-\hat{z}_0}\right), \tag{28}$$

with $U_m(x)$ being the mth Chebyshev polynomial of the second kind, we can finally arrive at

$$\sum_{m=0}^{N} c_m T_m(x)\left(\sqrt{1-x^2}+S_e m\right) - \frac{K}{M}\sum_{m=0}^{N}\sum_{j=1}^{M} c_m T_m(t_j)\sqrt{1-(t_j)^2}\left[1-\frac{\sqrt{(t_j+2\hat{d})^2-1}}{x+t_j+2\hat{d}}\right] = \frac{1}{\pi}\left(1+K+\mathrm{Re}\left\{\frac{\sqrt{\hat{z}_0^2-1}}{x-\hat{z}_0}\right\}+K\mathrm{Re}\left\{\frac{\sqrt{(\hat{z}_0+2\hat{d})^2-1}}{x+\hat{z}_0+2\hat{d}}\right\}\right). \tag{29}$$

The multi-valued functions $\sqrt{\hat{z}_0^2-1}$ and $\sqrt{(\hat{z}_0+2\hat{d})^2-1}$ in Eq. (29) should be judiciously chosen in the following manner: $\mathrm{Re}\left\{\sqrt{\hat{z}_0^2-1}\right\} > 0$ if $\mathrm{Re}\{\hat{z}_0\} > 0$, $\mathrm{Re}\left\{\sqrt{\hat{z}_0^2-1}\right\} < 0$ if $\mathrm{Re}\{\hat{z}_0\} < 0$; $\mathrm{Re}\left\{\sqrt{(\hat{z}_0+2\hat{d})^2-1}\right\} < 0$.

Meanwhile, the other unknown density function $\hat{f}(x)$ is approximated as

$$\hat{f}(x) = \frac{1}{\sqrt{1-x^2}}\sum_{m=0}^{N} d_m T_m(x), \tag{30}$$

where $d_m, m = 0, 1, 2, \ldots, N$ are $N+1$ unknown coefficients.

Substituting the above expression into Eq. (18), performing the complete and incomplete integrals and also considering the Gauss–Chebyshev integration formula, we finally arrive at

$$\frac{1}{S_e}d_0(\cos^{-1}x-\pi)+\sum_{m=1}^{N}d_m\left[U_{m-1}(x)+\frac{1}{S_e m}\sin(m\cos^{-1}x)\right]$$
$$+\frac{K}{M}\sum_{m=0}^{N}\sum_{j=1}^{M}\frac{d_m T_m(t_j)}{x+t_j+2\hat{d}}=-\frac{1}{\pi}\mathrm{Im}\left\{\frac{1}{x-\hat{z}_0}\right\}+\frac{K}{\pi}\mathrm{Im}\left\{\frac{1}{x+\hat{z}_0+2\hat{d}}\right\}, \tag{31}$$

where t_j has been defined in Eq. (22).

If we select the collocation points given by $x=-\cos\left(\frac{i\pi}{N}\right)$ for $i=1,2,\ldots,N$, Eqs. (29) and (31) together with Eq. (19) are further reduced to the following two sets of algebraic equations

$$\sum_{m=0}^{N}(-1)^m\cos\left(\frac{mi\pi}{N}\right)\left[\sin\left(\frac{i\pi}{N}\right)+S_e m\right]c_m$$
$$-\frac{K}{M}\sum_{m=0}^{N}\sum_{j=1}^{M}\cos\left(\frac{\pi m(2j-1)}{2M}\right)\sin\left(\frac{\pi(2j-1)}{2M}\right)$$
$$\times\left[1+\frac{\sqrt{\left[\cos\left(\frac{\pi(2j-1)}{2M}\right)+2\hat{d}\right]^2-1}}{\cos\left(\frac{i\pi}{N}\right)-\cos\left(\frac{\pi(2j-1)}{2M}\right)-2\hat{d}}\right]c_m$$
$$=\frac{1}{\pi}\left(1+K-\mathrm{Re}\left\{\frac{\sqrt{\hat{z}_0^2-1}}{\cos\left(\frac{i\pi}{N}\right)+\hat{z}_0}\right\}-K\mathrm{Re}\left\{\frac{\sqrt{(\hat{z}_0+2\hat{d})^2-1}}{\cos\left(\frac{i\pi}{N}\right)-\hat{z}_0-2\hat{d}}\right\}\right),\quad i=1,2,\ldots,N,$$
$$\sum_{m=0,m\neq1}^{N}\frac{1+(-1)^m}{1-m^2}c_m=0, \tag{32}$$
$$-\frac{d_0}{S_e}\frac{i\pi}{N}+\sum_{m=1}^{N}(-1)^{m-1}\sin\left(\frac{mi\pi}{N}\right)\left[\frac{1}{\sin\left(\frac{i\pi}{N}\right)}+\frac{1}{S_e m}\right]d_m$$
$$-\frac{K}{M}\sum_{m=0}^{N}\sum_{j=1}^{M}\frac{\cos\left(\frac{\pi m(2j-1)}{2M}\right)}{\cos\left(\frac{i\pi}{N}\right)-\cos\left(\frac{\pi(2j-1)}{2M}\right)-2\hat{d}}d_m$$
$$=\frac{1}{\pi}\mathrm{Im}\left\{\frac{1}{\cos\left(\frac{i\pi}{N}\right)+\hat{z}_0}\right\}-\frac{K}{\pi}\mathrm{Im}\left\{\frac{1}{\cos\left(\frac{i\pi}{N}\right)-\hat{z}_0-2\hat{d}}\right\},i=1,2,\ldots,N-1,$$
$$-\frac{d_0}{S_e}\pi+\sum_{m=1}^{N}m d_m+\frac{K}{M}\sum_{m=0}^{N}\sum_{j=1}^{M}\frac{\cos\left(\frac{\pi m(2j-1)}{2M}\right)}{1+\cos\left(\frac{\pi(2j-1)}{2M}\right)+2\hat{d}}d_m$$
$$=\frac{1}{\pi}\mathrm{Im}\left\{\frac{1}{-1+\hat{z}_0}\right\}+\frac{K}{\pi}\mathrm{Im}\left\{\frac{1}{1+\hat{z}_0+2\hat{d}}\right\},\quad d_0=0. \tag{33}$$

The Cauchy singular integro-differential equations in Eqs. (17)–(19) have been reduced to the linear algebraic equations in Eqs. (32) and (33). The $N+1$ coefficients $c_m, m=0,1,2,\ldots,N$ can be uniquely determined by solving Eq. (32), whilst the other $N+1$ coefficients $d_m, m=0,1,2,\ldots,N$ can be uniquely determined by solving Eq. (33).

5. The stress field and image force

By substituting the two analytic functions in Eq. (9) into Eq. (2), we obtain the stress field in the bimaterial as follows

$$\sigma_{32}^{(1)}+\mathrm{i}\sigma_{31}^{(1)}=\frac{1}{2\pi}\int_{d-a}^{d+a}\frac{\mu_1 b(\xi)-\mathrm{i}f(\xi)}{z-\xi}\mathrm{d}\xi+\frac{K}{2\pi}\int_{d-a}^{d+a}\frac{\mu_1 b(\xi)+\mathrm{i}f(\xi)}{z+\xi}\mathrm{d}\xi$$
$$+\frac{\mu_1 b_z}{2\pi(z-z_0)}+\frac{\mu_1 K b_z}{2\pi(z+\bar{z}_0)},\quad \mathrm{Re}\{z\}>0,$$
$$\sigma_{32}^{(2)}+\mathrm{i}\sigma_{31}^{(2)}=\frac{\mu_2(1-K)}{2\pi}\int_{d-a}^{d+a}\frac{b(\xi)-\mathrm{i}\mu_1^{-1}f(\xi)}{z-\xi}\mathrm{d}\xi+\frac{\mu_2(1-K)b_z}{2\pi(z-z_0)},\quad \mathrm{Re}\{z\}<0, \tag{34}$$

or equivalently in the following normalized form

$$\sigma_{32}^{(1)}+\mathrm{i}\sigma_{31}^{(1)}=\frac{\mu_1 b_z}{2\pi a}\int_{-1}^{1}\frac{\hat{b}(t)-\mathrm{i}\hat{f}(t)}{\hat{z}-t}\mathrm{d}t+\frac{\mu_1 b_z K}{2\pi a}\int_{-1}^{1}\frac{\hat{b}(t)+\mathrm{i}\hat{f}(t)}{\hat{z}+t+2\hat{d}}\mathrm{d}t$$
$$+\frac{\mu_1 b_z}{2\pi a(\hat{z}-\hat{z}_0)}+\frac{\mu_1 K b_z}{2\pi a(\hat{z}+\bar{\hat{z}}_0+2\hat{d})},\quad \mathrm{Re}\{\hat{z}\}>-\hat{d},$$
$$\sigma_{32}^{(2)}+\mathrm{i}\sigma_{31}^{(2)}=\frac{\mu_2 b_z(1-K)}{2\pi a}\int_{-1}^{1}\frac{\hat{b}(t)-\mathrm{i}\hat{f}(t)}{\hat{z}-t}\mathrm{d}t+\frac{\mu_2 b_z(1-K)}{2\pi a(\hat{z}-\hat{z}_0)},\quad \mathrm{Re}\{\hat{z}\}<-\hat{d}, \tag{35}$$

where $\hat{z}=z/a-\hat{d}$. It is seen in Eq. (35) that once the integrals in Eq. (35) are computed, the stresses can be arrived at. It can be deduced from Eqs. (17), (18) and (35) that the stresses exhibit both the weak logarithmic and the strong square root singularities at the two crack tips if $\mathrm{Im}\{\hat{z}_0\}\neq 0$, they exhibit only the weak logarithmic singularity at the two crack tips if $\mathrm{Im}\{\hat{z}_0\}=0$. The integrals in Eq. (35) can also be computed by the Gauss–Chebyshev integration formula.

By using the Peach–Koehler formula [4], the image force acting on the screw dislocation is given by

$$F_1-\mathrm{i}F_2=\frac{\mu_1 b_z^2}{2\pi a}\left[\int_{-1}^{1}\frac{\hat{b}(t)-\mathrm{i}\hat{f}(t)}{\hat{z}_0-t}\mathrm{d}t+K\int_{-1}^{1}\frac{\hat{b}(t)+\mathrm{i}\hat{f}(t)}{\hat{z}_0+t+2\hat{d}}\mathrm{d}t+\frac{K}{\hat{z}_0+\bar{\hat{z}}_0+2\hat{d}}\right], \tag{36}$$

where F_1 and F_2 are the force components along the x_1 and x_2 axes.

If $|\hat{z}_0|=r/a=\hat{r}\to\infty$ for the long-range interaction between the dislocation and the crack, the image force becomes

$$F_1-\mathrm{i}F_2=\begin{cases}\frac{\mu_1 b_z^2}{\pi a}\left[\frac{K}{2(\hat{z}_0+\bar{\hat{z}}_0)}-\frac{K\hat{d}}{(\hat{z}_0+\bar{\hat{z}}_0)^2}+\frac{\chi}{\hat{z}_0^2\bar{\hat{z}}_0}+\frac{\gamma}{\bar{\hat{z}}_0^3}\right], & \theta\neq\frac{\pi}{2},\frac{3\pi}{2},\\ \frac{\mu_1 b_z^2}{\pi a}\left[\frac{K}{4\hat{d}}+\frac{\mathrm{i}(\gamma-\chi)}{\hat{r}^3}\right], & \theta=\frac{\pi}{2},\\ \frac{\mu_1 b_z^2}{\pi a}\left[\frac{K}{4\hat{d}}-\frac{\mathrm{i}(\gamma-\chi)}{\hat{r}^3}\right], & \theta=\frac{3\pi}{2},\end{cases} \tag{37}$$

where the two real coefficients ξ and γ are defined by

$$\chi=-\frac{1}{4\pi}\int_{-1}^{1}t\left[(K-1)^2\tilde{b}(t)-(K+1)^2\tilde{f}(t)\right]\mathrm{d}t,$$
$$\gamma=-\frac{1}{4\pi}\int_{-1}^{1}t\left[(K-1)^2\tilde{b}(t)+(K+1)^2\tilde{f}(t)\right]\mathrm{d}t. \tag{38}$$

In Eq. (38), the two functions $\tilde{b}(x)$ and $\tilde{f}(x)$ are determined by solving the following Cauchy singular integro-differential equations:

$$-\frac{1}{\pi}\int_{-1}^{1}\frac{\tilde{b}(t)}{t-x}\mathrm{d}t+\frac{K}{\pi}\int_{-1}^{1}\frac{\tilde{b}(t)}{x+t+2\hat{d}}\mathrm{d}t+1=S_e\tilde{b}'(x),\ -1<x<1,$$
$$\int_{-1}^{1}\tilde{b}(t)\mathrm{d}t=0, \tag{39}$$

$$\frac{1}{\pi}\int_{-1}^{1}\frac{\tilde{f}(t)}{t-x}\mathrm{d}t+\frac{K}{\pi}\int_{-1}^{1}\frac{\tilde{f}(t)}{x+t+2\hat{d}}\mathrm{d}t-\frac{1}{S_e}\int_{-1}^{x}\tilde{f}(t)\mathrm{d}t=1,\ -1<x<1,$$
$$\int_{-1}^{1}\tilde{f}(t)\mathrm{d}t=0. \tag{40}$$

6. A Zener–Stroh crack perpendicular to the interface

In the above discussions, we have in fact assumed that the finite crack is a Griffith one which satisfies Eq. $(16)_1$. In this section, we will first consider a Zener–Stroh crack loaded by the net screw dislocation Burgers vector b_T (see [7] and the references cited therein). The problem configuration is very similar to that discussed in Sect. 3 now with the assumption that $b_z=0$. In this loading case, it is found that the line force density is zero, i.e., $f(x_1)=0$. The dislocation density $b(x_1)$ should satisfy the following Cauchy singular integro-differential equation

$$-\frac{\mu_1}{\pi}\int_{d-a}^{d+a}\frac{b(\xi)}{\xi-x_1}\mathrm{d}\xi+\frac{K\mu_1}{\pi}\int_{d-a}^{d+a}\frac{b(\xi)}{\xi+x_1}\mathrm{d}\xi=(\mu^s-\sigma_0)b'(x_1), d-a<x_1<d+a, \tag{41}$$

and the auxiliary condition

$$\int_{d-a}^{d+a}b(\xi)\mathrm{d}\xi=b_T. \tag{42}$$

By introducing $x=(x_1-d)/a$ and $t=(\xi-d)/a$, Eqs. (41) and (42) can be rewritten into the following normalized form

$$-\frac{1}{\pi}\int_{-1}^{1}\frac{\hat{b}(t)}{t-x}\mathrm{d}t+\frac{K}{\pi}\int_{-1}^{1}\frac{\hat{b}(t)}{x+t+2\hat{d}}\mathrm{d}t=S_e\hat{b}'(x),\ -1<x<1, \tag{43}$$

$$\int_{-1}^{1}\hat{b}(t)\mathrm{d}t=1, \tag{44}$$

where $\hat{d}$ and S_e have been defined in Eq. (20), whereas $\hat{b}(x)$ is redefined as follows

$$\hat{b}(x)=\frac{ab(x)}{b_T}. \tag{45}$$

We can also expand $\hat{b}(x)$ into Eq. (26). Consequently, the $N+1$ coefficients $c_m, m=0,1,2,\ldots,N$ in the expansion can be uniquely determined by solving the following se of algebraic equations

$$\sum_{m=0}^{N}(-1)^m\cos\left(\frac{mi\pi}{N}\right)\left[\sin\left(\frac{i\pi}{N}\right)+S_e m\right]c_m$$
$$-\frac{K}{M}\sum_{m=0}^{N}\sum_{j=1}^{M}\cos\left(\frac{\pi m(2j-1)}{2M}\right)\sin\left(\frac{\pi(2j-1)}{2M}\right)\left[1+\frac{\sqrt{\left[\cos\left(\frac{\pi(2j-1)}{2M}\right)+2\hat{d}\right]^2-1}}{\cos\left(\frac{i\pi}{N}\right)-\cos\left(\frac{\pi(2j-1)}{2M}\right)-2\hat{d}}\right]c_m$$
$$=\frac{1}{\pi}, i=1,2,\ldots,N,\quad \sum_{m=0,m\neq 1}^{N}\frac{1+(-1)^m}{1-m^2}c_m=1. \tag{46}$$

In the case of a Zener–Stroh crack, the stresses exhibit only the weak logarithmic singularity at the two crack tips.

According to the classification of dislocation–crack interaction by [31,32], the screw dislocation can be emitted from the finite crack or originated from elsewhere. It is apparent that the analyses in Sects. 3 and 4 are valid for the latter case in which the screw dislocation is originated from a source other than the crack. If the screw dislocation is emitted from the crack, its solution can be obtained as the superposition of that obtained in Sects. 3 and 4 and that for a Zener–Stroh crack solved in this section. Now $b_T=-b_z$ in order to ensure that a Burger circuit enclosing both the crack and the dislocation will be closed [31,32]. In particular, if $|\hat{z}_0|\to\infty$ for the long-range interaction, the image force on the dislocation becomes

$$F_1-\mathrm{i}F_2=\frac{\mu_1 b_z^2}{\pi a}\left(-\frac{K+1}{2\hat{z}_0}+\frac{\eta}{\hat{z}_0^2}\right)+F_{1g}-\mathrm{i}F_{2g}, \tag{47}$$

where $F_{1g}-\mathrm{i}F_{2g}$ is just the expression of $F_1-\mathrm{i}F_2$ in Eq. (37) for a dislocation originated from elsewhere, and the real coefficient η is defined by

$$\eta=\frac{K-1}{2}\int_{-1}^{1}t\hat{b}(t)\mathrm{d}t, \tag{48}$$

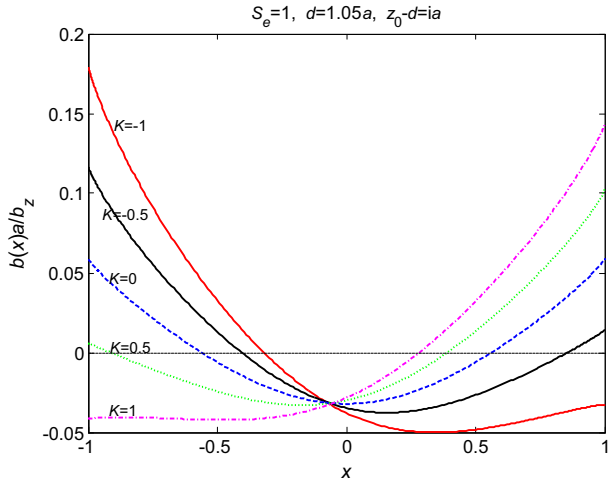

FIG. 2. Dislocation density $b(x)$ for different values of $K=-1,-0.5,0,0.5,1$ with $S_e=1,\hat{d}=1.05,\hat{z}_0=\mathrm{i}$. The crack is a Griffith crack

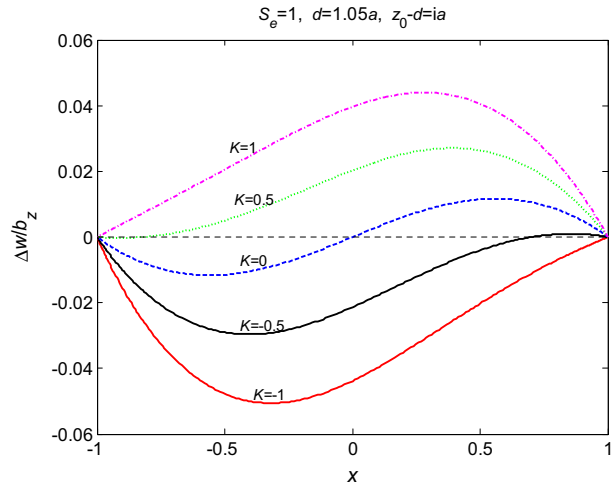

FIG. 3. The crack opening displacement $\Delta w = -a\int_{-1}^{x} b(t)\mathrm{d}t$ for different values of $K = -1, -0.5, 0, 0.5, 1$ with $S_e = 1, \hat{d} = 1.05, \hat{z}_0 = \mathrm{i}$. The crack is a Griffith crack

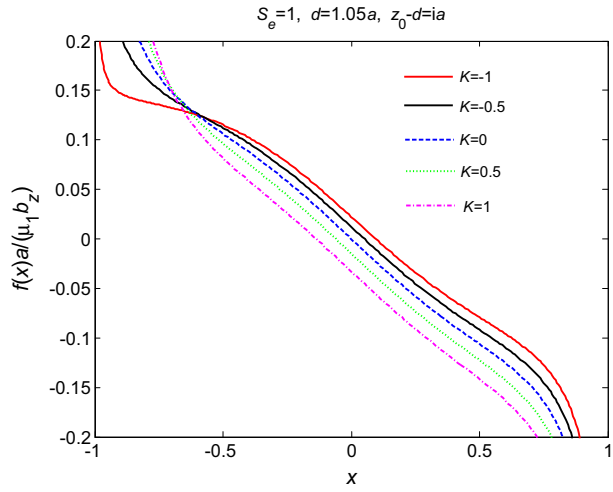

FIG. 4. Line force density $f(x)$ for different values of $K = -1, -0.5, 0, 0.5, 1$ with $S_e = 1, \hat{d} = 1.05, \hat{z}_0 = \mathrm{i}$. The crack is a Griffith crack

with the function $\hat{b}(x)$ being determined by solving the Cauchy singular integro-differential equation in Eqs (43) and (44).

7. Numerical results and discussions

During the calculation, we choose $N = 300$ and $M = 15$. When the screw dislocation is extremely close to the crack faces, a sufficiently large number of points on the segment $[-1, 1]$ is required to compute the first integral in Eq. (36) by using the Gauss–Chebyshev integration formula. As a check, when $K = 0$, the current numerical result just recovers that in [26] for a screw dislocation interacting with a Griffith crack

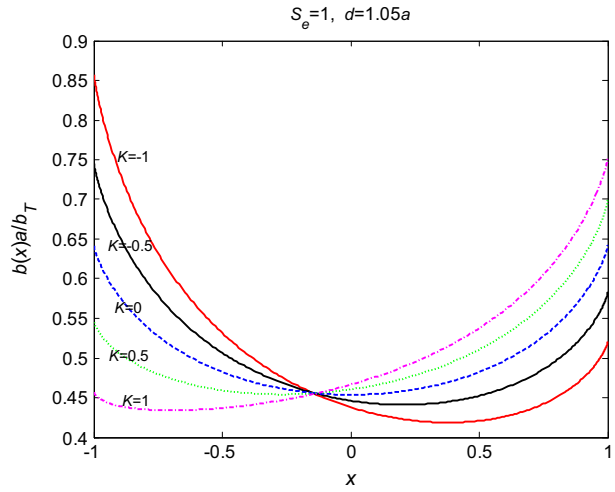

FIG. 5. Dislocation density $b(x)$ on a Zener–Stroh crack for different values of $K = -1, -0.5, 0, 0.5, 1$ with $S_e = 1, \hat{d} = 1.05$

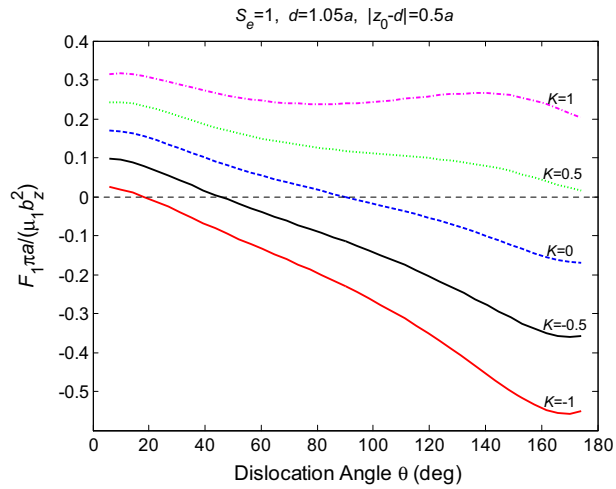

FIG. 6. Image force component F_1 versus the dislocation angle θ for five different values of $K = -1, -0.5, 0, 0.5, 1$ with $S_e = 1, \hat{d} = 1.05, |\hat{z}_0| = 0.5$. The dislocation is originated from a source other than the crack

in a homogeneous solid. Illustrated in Figs. 2, 3 and 4 are the dislocation density $b(x)$, the crack opening displacement $\Delta w = -a\int_{-1}^{x} b(t)\mathrm{d}t$ and the line force density $f(x)$ for different values of the mismatch parameter K with $S_e = 1, \hat{d} = 1.05$ and $\hat{z}_0 = \mathrm{i}$. The results in the three figures are obtained from Eqs. (32) and (33) for a dislocation originated from a source other than the crack. As clearly seen in Fig. 2, $b(x)$ is finite at $x = \pm 1$ due to the incorporation of surface elasticity. As a result, the crack-tip opening angles in Fig. 3 are always strictly less than $\pi/2$. The mismatch parameter K exerts a significant influence on both $b(x)$ and Δw. Our detailed results show that $b(-1) = 0$ when $K = 0.56$. In this case, the opening angle at the left crack tip is zero and the stresses only exhibit the square root singularity at the left crack tip. Similarly, it is found that $b(+1) = 0$ when $K = -0.65$. In this case, the opening angle at the

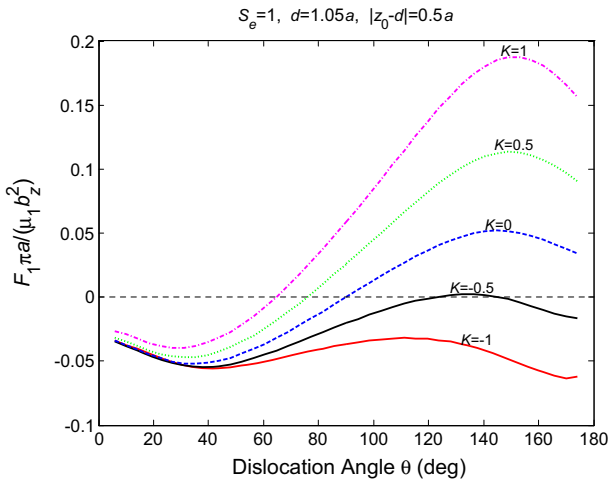

FIG. 7. Image force component F_1 versus the dislocation angle θ for five different values of $K = -1, -0.5, 0, 0.5, 1$ with $S_e = 1, \hat{d} = 1.05, |\hat{z}_0| = 0.5$. The dislocation is emitted from the crack

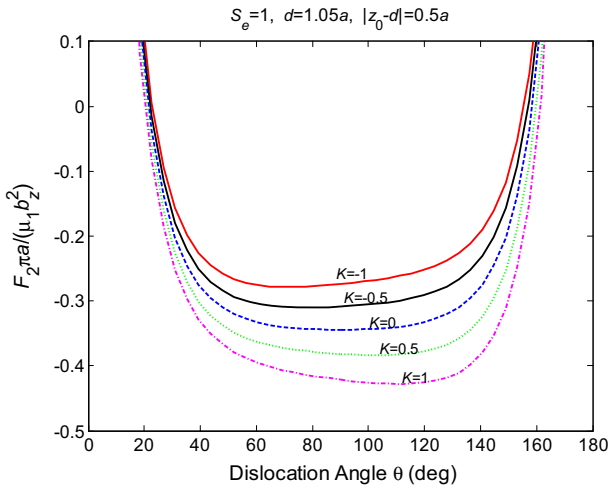

FIG. 8. Image force component F_2 versus the dislocation angle θ for five different values of $K = -1, -0.5, 0, 0.5, 1$ with $S_e = 1, \hat{d} = 1.05, |\hat{z}_0| = 0.5$. The dislocation is emitted from the crack

right crack tip is zero and the stresses only exhibit the square root singularity at the right crack tip. It is observed from Fig. 3 that Δw at a fixed position x is an increasing function of K.

We show in Fig. 5 the dislocation density $b(x)$ distributed on a Zener–Stroh crack by solving Eq. (46) for different values of the mismatch parameter K with $S_e = 1$ and $\hat{d} = 1.05$. Different from the result in Fig. 2 for a Griffith crack, $\hat{b}(x)$ in Fig. 5 is always positive. When $K = 0$, $\hat{b}(x)$ is symmetric with respect to $x = 0$. When $K > 0$, $\hat{b}(x)$ is suppressed in the left portion and is enlarged in the right portion. When $K < 0$, $\hat{b}(x)$ is enlarged in the left portion and is suppressed in the right portion.

Figure 6 illustrates the image force component F_1 as a function of the dislocation angle for different values of the mismatch parameter K with $S_e = 1, \hat{d} = 1.05$ and $|\hat{z}_0| = 0.5$. The dislocation is originated from a source other than the crack. It is observed from Fig. 6 that the value of F_1 at a fixed dislocation

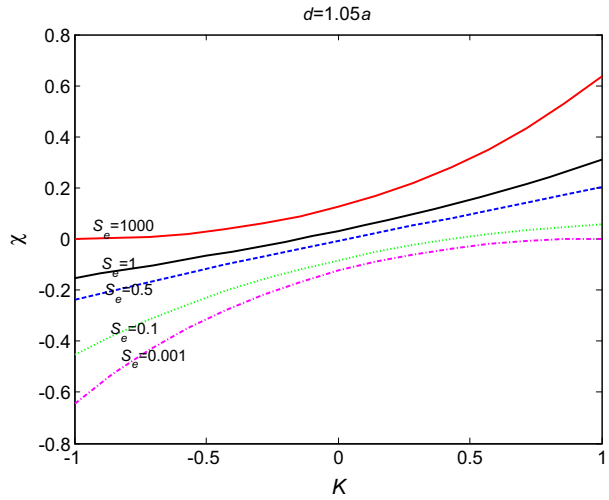

FIG. 9. Values of ξ defined in Eq. (38) for different combinations of K and S_e with $\hat{d} = 1.05$.

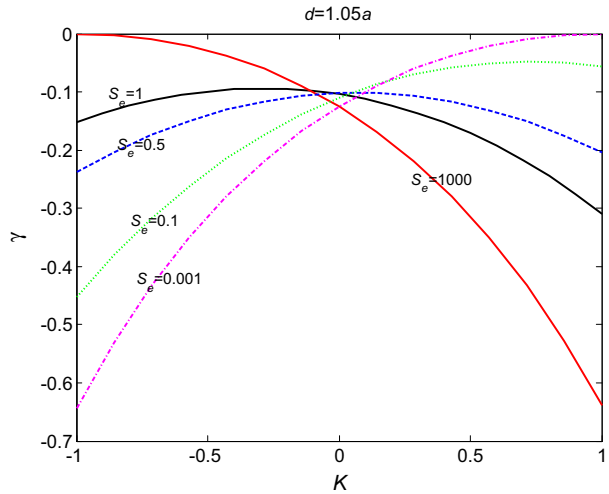

FIG. 10. Values of γ defined in Eq. (38) for different combinations of K and S_e with $\hat{d} = 1.05$

angle monotonically increases with the increase in K. The dislocation is repelled from the interface (i.e., $F_1 > 0$) for the whole range of the dislocation angle when $K = 0.5, 1$. The dislocation is attracted to the interface (i.e., $F_1 < 0$) for the majority of the dislocation angle ($20^\circ < \theta < 180^\circ$) when $K = -1$ for a free surface. The influence of K on F_2 is not as apparent as that on F_1. Our results indicate that with this set of parameters, the dislocation is always repelled from the crack ($F_2 > 0$) for the whole range of the dislocation angle. The dislocation–crack repulsion is solely caused by the incorporation of the surface elasticity on the crack surface because the dislocation will be attracted to the crack without surface effect.

We show in Figs. 7 and 8 the image force components F_1 and F_2 on a dislocation emitted from the crack as functions of the dislocation angle for different values of the mismatch parameter K with $S_e = 1, \hat{d} = 1.05$ and $|\hat{z}_0| = 0.5$. A comparison of Fig. 6 with Fig. 7 reveals that the results for the two

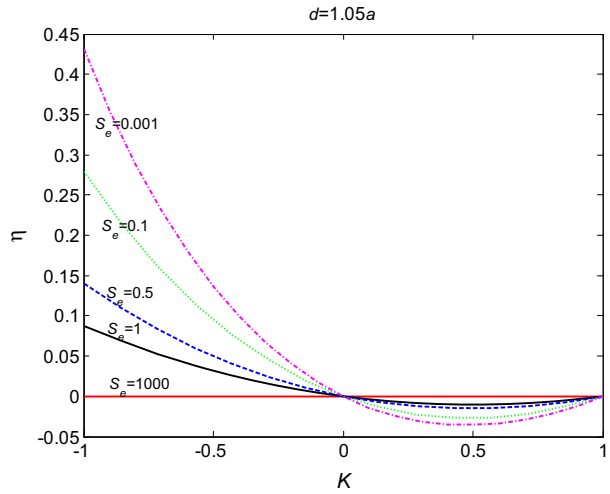

FIG. 11. Variation of η defined in Eq. (48) as a function of K and S_e with $\hat{d} = 1.05$

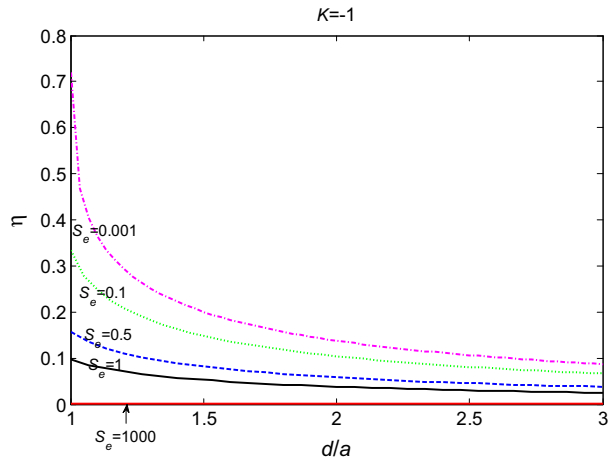

FIG. 12. Variation of η defined in Eq. (48) as a function of $\hat{d}$ and S_e with $K = -1$

cases are quite different. The magnitude of F_1 on a dislocation emitted from the crack is much lower than that on a dislocation originated from elsewhere. As shown in Fig. 8, the influence of K on F_2 is also significant when the dislocation is emitted from the crack, a phenomenon different from the case when the dislocation is originated from elsewhere. It is also observed from Fig. 8 that the dislocation is repelled from the crack ($F_2 > 0$) when it is close enough to the crack incorporating surface elasticity, and the dislocation is attracted to the crack ($F_2 < 0$) when it is far enough from the crack. A stiffer phase 2 ($K > 0$) will enlarge the attraction region and suppress the repulsion region. On the other hand, a softer phase 2 ($K < 0$) will suppress the attraction region and enlarge the repulsion region.

Finally, we present the results for the long-range interaction between the dislocation and the crack. We show in Figs. 9 and 10 the values of the two real coefficients ξ and γ defined in Eq. (38) for different combinations of K and S_e with $\hat{d} = 1.05$. It is observed that γ is always negative, whereas the sign of χ is dependent on the specific combination of K and S_e. For example, $\chi < 0$ for any value of K when

$S_e = 0.001$, $\chi > 0$ for any value of K when $S_e = 1000$. We show in Fig. 11 the variation of η defined in Eq. (48) as a function of K and S_e with $\hat{d} = 1.05$. When $K = 0$ or $K = 1$, η is always zero for any value of S_e. When $K = -1$, the influence of S_e on η is most significant. Figure 12 further shows the variation of η as a function of $\hat{d}$ and S_e with $K = -1$. It is seen that η is a decreasing function of both $\hat{d}$ and S_e, η decays to zero as $\hat{d} \to \infty$ and $\eta \approx 0$ when $S_e = 1000$.

8. Conclusions

In this paper, we have investigated the interaction problem associated with a screw dislocation near a mode III finite crack with surface elasticity perpendicular to a bimaterial interface. In our discussion, the screw dislocation can be originated from a source other than the crack (Sects. 3, 4), or it can be emitted from the crack (Sect. 5). The problem of a Zener–Stroh crack perpendicular to a bimaterial interface is also solved in Sect. 5. By using the Green's function method, the interaction problem is finally reduced to two decoupled first-order Cauchy singular integro-differential equations. Consequently, a complete solution has been derived. The image force acting on the screw dislocation is also obtained. Detailed numerical results are presented to demonstrate the effects of the mismatch parameter and surface elasticity on the screw dislocation density and line force density on the crack, and on the material force acting on the screw dislocation.

Acknowledgements

This work was supported by the National Natural Science Foundation of China (Grant No: 11272121).

References

1. Antipov, Y.A., Schiavone, P.: Integro-differential equation for a finite crack in a strip with surface effects. Q. J. Mech. Appl. Math. **64**, 87–106 (2011)
2. Chakrabarti, A. Hamsapriye: Numerical solution of a singular integro-differential equation. Z. Angew. Math. Mech. **79**, 233–241 (1999)
3. Chen, T., Dvorak, G.J., Yu, C.C.: Size-dependent elastic properties of unidirectional nano-composites with interface stresses. Acta Mech. **188**, 39–54 (2007)
4. Dundurs J.: Elastic interaction of dislocations with inhomogeneities. In: Mura, T. (eds.) Mathematical Theory of Dislocations, pp. 70–115. ASME, New York (1969).
5. Erdogan, F.: Fracture problems in composite materials. Eng. Fract. Mech. **4**, 811–840 (1972)
6. Erdogan, F., Gupta, G.D.: On the numerical solution of singular integral equations. Q. Appl. Math. **29**, 525–534 (1972)
7. Fan, H., Xiao, Z.M.: A Zener–Stroh crack near an interface. Int. J. Solids Struct. **34**, 2829–2842 (1997)
8. Gurtin, M.E., Murdoch, A.: A continuum theory of elastic material surfaces. Arch. Ration. Mech. Anal. **57**, 291–323 (1975)
9. Gurtin, M.E., Murdoch, A.I.: Surface stress in solids. Int. J. Solids Struct. **14**, 431–440 (1978)
10. Gurtin, M.E., Weissmuller, J., Larche, F.: A general theory of curved deformable interface in solids at equilibrium. Philos. Mag. A **78**, 1093–1109 (1998)
11. Kim, C.I., Ru, C.Q., Schiavone, P.: A clarification of the role of crack-tip conditions in linear elasticity with surface effects. Math. Mech. Solids **18**, 59–66 (2013)
12. Kim, C.I., Schiavone, P., Ru, C.Q.: The effects of surface elasticity on an elastic solid with mode-III crack: complete solution. ASME J. Appl. Mech. **77**, 021011-1–021011-7 (2010)
13. Kim, C.I., Schiavone, P., Ru, C.Q.: Analysis of a mode III crack in the presence of surface elasticity and a prescribed non-uniform surface traction. Z. Angew. Math. Phys. **61**, 555–564 (2010)
14. Kim, C.I., Schiavone, P., Ru, C.Q.: Analysis of plane-strain crack problems (mode I and mode II) in the presence of surface elasticity. J. Elast. **104**, 397–420 (2011)
15. Kim, C.I., Schiavone, P., Ru, C.Q.: The effects of surface elasticity on mode-III interface crack. Arch. Mech. **63**, 267–286 (2011)

16. Kim, C.I., Schiavone, P., Ru, C.Q.: Effect of surface elasticity on an interface crack in plane deformations. Proc. R. Soc. Lond. A **467**, 3530–3549 (2011)
17. Kwon, J.H., Lee, K.Y.: Electromechanical effects of a screw dislocation around a finite crack in a piezoelectric material. ASME J. Appl. Mech. **69**, 55–62 (2002)
18. Markenscoff, X., Dundurs, J.: Annular inhomogeneities with eigenstrain and interphase modeling. J. Mech. Phys. Solids **64**, 468–482 (2014)
19. Ru, C.Q.: Simple geometrical explanation of Gurtin–Murdoch model of surface elasticity with clarification of its related versions. Sci. China **53**, 536–544 (2010)
20. Steigmann, D.J., Ogden, R.W.: Plane deformations of elastic solids with intrinsic boundary elasticity. Proc. R. Soc. Lond. A **453**, 853–877 (1997)
21. Suo, Z.: Singularities interacting with interfaces and cracks. Int. J. Solids Struct. **25**, 1133–1142 (1989)
22. Suo, Z.G.: Singularities, interfaces and cracks in dissimilar anisotropic media. Proc. R. Soc. Lond. A **427**, 331–358 (1990)
23. Ting, T.C.T.: Image singularities of Green's functions for anisotropic elastic half-spaces and bimaterials. Q. J. Mech. Appl. Math. **45**, 119–139 (1992)
24. Ting, T.C.T.: Anisotropic Elasticity-Theory and Applications. Oxford University Press, New York. (1996)
25. Wang, X.: A mode III arc shaped crack with surface elasticity. Z. Angew. Math. Phys. **66**, 1987–2000 (2015)
26. Wang, X., Fan, H.: Interaction between a nanocrack with surface elasticity and a screw dislocation. Math. Mech. Solids (2015). doi:10.1177/1081286515574147
27. Wang, X., Schiavone, P.: Interaction between an edge dislocation and a crack with surface elasticity. ASME J. Appl. Mech. **82**, 021006-1–021006-8 (2015)
28. Wang, X., Zhou, K.: A crack with surface effects in a piezoelectric material. Math. Mech. Solids (2015). doi:10.1177/1081286514568907
29. Wang, X., Zhou, K., Wu, M.S.: Interface cracks with surface elasticity in anisotropic bimaterials. Int. J. Solids Struct. **59**, 110–120 (2015)
30. Yi, D.K., Xiao, Z.M., Tan, S.K.: Elastic and plastic fracture analysis of a crack perpendicular to an interface between dissimilar materials. Acta Mech. **223**, 1031–1045 (2012)
31. Zhang, T.Y., Li, J.C.M.: Image forces and shielding effects of a screw dislocation near a finite-length crack. Mater. Sci. Eng. A **142**, 35–39 (1991)
32. Zhang, T.Y., Li, J.C.M.: Image forces and shielding effects of an edge dislocation near a finite length crack. Acta Metall. **39**, 2739–2744 (1991)

Xu Wang
School of Mechanical and Power Engineering
East China University of Science and Technology
130 Meilong Road
Shanghai
200237
China
e-mail: xuwang@ecust.edu.cn

(Received: August 15, 2015)